Constellations on the Sphere with Efficient Encoding-Decoding for Noncoherent Communications

Diego Cuevas, Javier Álvarez-Vizoso, Carlos Beltrán, Ignacio Santamaría, *Senior Member, IEEE*, Vít Tuček, and Gunnar Peters

***Abstract*—In this paper, we propose a new structured Grassmannian constellation for noncoherent communications over single-input multiple-output (SIMO) Rayleigh block-fading channels. The constellation, which we call Grass-Lattice, is based on a measure preserving mapping from the unit hypercube to the Grassmannian of lines. The constellation structure allows for on-the-fly symbol generation, low-complexity decoding, and simple bit-to-symbol Gray-like coding. Simulation results show that Grass-Lattice has symbol and bit error rate performance close to that of a numerically optimized unstructured constellation, and is more power efficient than other structured constellations proposed in the literature and a coherent pilot-based scheme.**

***Index Terms*—Noncoherent communications, Grassmannian constellations, SIMO channels, measure-preserving mapping.**

I. Introduction

In communications over fading channels, it is usually assumed that the channel state information (CSI) is typically estimated at the receiver side by periodic transmission of a few known pilots and then it is used for decoding at the receiver and/or for precoding at the transmitter. These are known as coherent schemes. The channel capacity for coherent systems is known to increase linearly with the minimum number of transmit and receive antennas at high signal-to-noise (SNR) ratio [1], [2] when the channel remains approximately constant over a long coherence time (slowly fading scenarios).

However, in fast fading scenarios or massive multiple-input multiple-output (MIMO) systems for ultra-reliable low-latency communications (URLLC), to obtain an accurate channel estimate would require pilots to occupy a disproportionate fraction of communication resources [3], [4]. These new scenarios that have emerged with 5G and B5G systems motivate the use of noncoherent communications schemes in which neither the transmitter nor the receiver have any knowledge about the instantaneous CSI.

Despite the receiver not having CSI, a significant fraction of the coherent capacity can be achieved in noncoherent communication systems when the signal-to-noise ratio (SNR) is high, as shown in [5]–[8]. For the case of single-input multiple-output (SIMO) channels, which is the one we focus on in this paper, these works proved that at high SNR under additive Gaussian noise, assuming a Rayleigh block-fading SIMO channel with coherence time $T \geq 2$, the optimal strategy achieving the capacity is to transmit isotropically distributed unitary vectors belonging to the Grassmannian of lines or projective space [7], [8]. Equivalently, these constellations correspond to packings on the sphere. Therefore, in noncoherent SIMO communication systems the information is carried by the column span of the transmitted vector, which is not affected by the SIMO channel.

An extensive research has been conducted on the design of noncoherent constellations as optimal packings on the Grassmann manifold [9]–[23]. Some experimental evaluation of Grassmannian constellations in noncoherent communications using over-the-air transmission has been reported in [24]. Existing constellation designs can be generically categorized into two groups: structured or unstructured. Among the unstructured designs we can mention the alternating projection method [10], the numerical methods in [11]–[14], which optimize certain distance measures on the Grassmannian (e.g., chordal or spectral), and the methods proposed in [15] and [16], which maximize the so-called diversity product [25].

On the other side, structured designs impose some kind of structure on the constellation points, facilitating low complexity constellation mapping and demapping. This is achieved through algebraic constructions such as the Fourier-based constellation in [17], the uniquely factorable constellations in [18] or the analog subspace codes recently proposed in [19], designs based on group representations [20], [21], parameterized mappings of unitary matrices such as the Exp-Map design in [22] or structured partitions of the Grassmannian like the recently proposed Cube-Split constellation [23]. The Cube-Split constellation is of particular interest for this work as it is the design most related to our proposal. Cube-Split is based on a mapping from the unit hypercube to the Grassmann manifold

This work was supported by Huawei Technologies, Sweden under the project GRASSCOM. The work of D. Cuevas was also partly supported under grant FPU20/03563 funded by Ministerio de Universidades (MIU), Spain. The work of Carlos Beltrán was also partly supported under grant PID2020-113887GB-I00 funded by MCIN/ AEI /10.13039/501100011033. The work of I. Santamaria was also partly supported under grant PID2019-104958RB-C43 (ADELE) funded by MCIN/ AEI /10.13039/501100011033. A short preliminary version of this paper was presented at the 2022 IEEE Global Communications Conference: Signal Processing for Communications (Globecom 2022 SPC).

D. Cuevas, J. Álvarez Vizoso and I. Santamaria are with the Department of Communications Engineering, Universidad de Cantabria, 39005 Santander, Spain (e-mail: diego.cuevas@unican.es; javier.alvarezvizoso@unican.es; i.santamaria@unican.es).

C. Beltrán is with the Department of Mathematics, Statistics and Computing, Universidad de Cantabria, 39005 Santander, Spain (e-mail: carlos.beltran@unican.es).

V. Tuček and G. Peters are with the Department of Wireless Algorithms, Huawei Technologies, 16440 Kista, Sweden (email: vit.tucek@huawei.com; gunnar.peters@huawei.com)

such that the constellation points are distributed approximately uniformly on the Grassmannian. However, the Cube-Split mapping only achieves uniformly distributed points for $T = 2$. When $T > 2$, Cube-Split ignores the statistical dependencies between the components of the constellation points and applies the same mapping derived for $T = 2$. These limitations are overcome with our proposed mapping, named Grass-Lattice, which is a *measure preserving mapping* between the unit hypercube and the Grassmannian for any value of $T \geq 2$. The fact that the Grass-Lattice mapping is measure preserving guarantees that any set of points uniformly distributed in the input space (the hypercube), is mapped onto another set of points uniformly distributed in the output space (the Grassmann manifold). The constellation structure allows for on-the-fly symbol generation, low-complexity decoding, and simple bit-to-symbol Gray-like coding. There exist other ways of obtaining uniformly distributed points in the Grassmannian, e.g. by using random Gaussian matrices [26], but the resulting constellations would not have any kind of structure and would make it necessary to apply an exhaustive detector.

This paper extends the work presented in [27], which presents an overview of the Grass-Lattice constellation for SIMO channels. The proposed constellation is based on the composition of three mappings, which together produce a measure preserving mapping of the unit hypercube to the Grassmannian of lines. The first mapping transforms points uniformly distributed in the unit hypercube to normally distributed points. Then, the second mapping takes these normally distributed points and maps them to points uniformly distributed in the unit ball, which is the subset of vectors with modulus less than 1. Finally, the third mapping maps these uniformly distributed points in the unit ball to points uniformly distributed in the Grassmannian of lines. The novelties presented in this paper are the following:

- We present an alternative way of constructing the output vector in the second mapping, which transforms normally distributed points to points uniformly distributed in the unit ball, using a chi-squared random variable.
- We now derive the third mapping, which takes points uniformly distributed in the unit ball and maps them to points uniformly distributed in the Grassmannian of lines, for any number of transmit antennas. This is a first step to extend the Grass-Lattice mapping to the MIMO case, which is not straightforward since the corresponding target space (the Grassmann manifold of higher-dimensional subspaces) does not share the symmetry properties of projective space.
- We provide a visualization of the inputs and outputs of each mapping for the case $T = 2$.
- We include more comprehensive simulation results showing the symbol and bit error rate (SER and BER) performance as a function of the length of the lattice used in the input space, α.
- We also propose a new way of computing the optimum value of α based on the minimum chordal distance of the constellation.
- We include as a baseline the performance of a coherent pilot-based scheme in terms of SER, BER, and spectral efficiency versus energy per bit to noise power spectral density ratio (E_b/N_0).

The remainder of this paper is organized as follows. The system model is presented in Section II. In Section III we describe the proposed measure preserving mapping, named Grass-Lattice, which maps points uniformly distributed in the unit hypercube to the Grassmann manifold. We next present the procedures for encoding and decoding using Grass-Lattice mapping in Section IV. A comprehensive set of numerical simulation results to assess the performance of the proposed method in terms of symbol and bit error rates, as well as power efficiency, is provided in Section V. Finally, Section VI concludes the paper. In addition, the paper contains a set of appendices that includes the proofs of the mathematical results.

Notation: Matrices are denoted by bold-faced upper case letters, column vectors are denoted by bold-faced lower case letters, and scalars are denoted by light-faced lower case letters. The Euclidean norm is denoted by $\|\mathbf{v}\|$, the operator norm is denoted by $\|\mathbf{M}\|_{op}$ and j denotes the imaginary unit. The superscripts $(\cdot)^{\mathrm{T}}$ and $(\cdot)^{\mathrm{H}}$ denote transpose and Hermitian conjugate, respectively. We denote by $\mathbf{I}_n$ the identity matrix of size $n \times n$. A complex proper Gaussian distribution with zero mean and unit variance is denoted as $\mathcal{CN}(0,1)$ and $\mathbf{x} \sim \mathcal{CN}(\mathbf{0}, \mathbf{R})$ denotes a complex Gaussian vector in $\mathbb{C}^n$ with zero mean and covariance matrix $\mathbf{R}$. For real variables we use $\mathbf{x} \sim \mathcal{N}(\mathbf{0}, \mathbf{R})$. The complex Grassmann manifold of M-dimensional subspaces of the T-dimensional complex vector space $\mathbb{C}^T$ is denoted as $\mathbb{G}(M, \mathbb{C}^T)$. Particularly, the Grassmannian of lines $\mathbb{G}\left(1, \mathbb{C}^T\right)$, also called the complex projective space, is the space of one-dimensional subspaces in $\mathbb{C}^T$. Points in $\mathbb{G}(M, \mathbb{C}^T)$ are denoted as $[\mathbf{X}]$ and points in $\mathbb{G}\left(1, \mathbb{C}^T\right)$ are denoted as $[\mathbf{x}]$. For required background material on the Grassmann manifold we refer the reader to [28, Chap. 9].

II. System Model

A. System Model

We consider a noncoherent SIMO communication system where a single-antenna transmitter sends information to a receiver equipped with N antennas over a frequency-flat block-fading channel with coherence time T symbol periods. It is assumed that $T \geq 2$. Hence, the channel vector $\mathbf{h} \in \mathbb{C}^N$ stays constant during each coherence block of T symbols, and changes in the next block to an independent realization. The SIMO channel is assumed to be Rayleigh with no correlation at the receiver, i.e., $\mathbf{h} \sim \mathcal{CN}\left(0, \mathbf{I}_N\right)$, and unknown to both the transmitter and the receiver.

Within a coherence block the transmitter sends a signal $\mathbf{x} \in \mathbb{C}^T$ (which is taken from a finite constellation $\mathcal{C}$), normalized as $\mathbf{x}^H\mathbf{x} = 1$, that is a unitary basis for the one-dimensional subspace $[\mathbf{x}]$ in $\mathbb{G}\left(1, \mathbb{C}^T\right)$. The signal at the receiver $\mathbf{Y} \in \mathbb{C}^{T\times N}$ is

$$\mathbf{Y} = \mathbf{x}\mathbf{h}^{\mathrm{T}} + \sqrt{\frac{1}{T\rho}}\mathbf{W}, \tag{1}$$

where $\mathbf{W} \in \mathbb{C}^{T\times N}$ represents the additive Gaussian noise, with entries modeled as $w_{ij} \sim \mathcal{CN}(0,1)$, and ρ represents the signal-to-noise-ratio (SNR).

In a noiseless situation, Grassmannian signaling guarantees error-free detection without CSI because $\mathbf{x}$ and the noise-free vector on a receive antenna $\mathbf{y} = \mathbf{x}h$ represent the same point in $\mathbb{G}(1,\mathbb{C}^T)$. When the noise is present, the span of the received signal at each receive antenna deviates from that of $\mathbf{x}$ since the columns of $\mathbf{W}$ are almost surely not aligned with $\mathbf{x}$. This leads to a detection error if $\mathbf{Y}$ lies outside the decision region of the transmitted symbol.

The constellation $\mathcal{C}$ should be designed to minimize the probability of decoding error. This probability of error can be bounded by the pairwise error probability (PEP) union bound (UB). As it was shown in [6], the PEP decreases with the chordal distance between constellation points. Therefore, maximizing the pairwise chordal distance minimizes the union bound. This leads to the commonly used constellation design criteria of maximizing the minimum pairwise chordal distance. This optimization problem can be solved numerically but the resulting constellation is hard to exploit in practice due to its lack of structure.

For unstructured Grasmmannian constellations, the optimal Maximum Likelihood (ML) detector that minimizes the probability of error is given by

$$\tilde{\mathbf{x}} = \arg\max_{\mathbf{x}\in\mathcal{C}} \|\mathbf{Y}^{\mathrm{H}}\mathbf{x}\|^2, \tag{2}$$

where $\mathcal{C}$ represents the set of K constellation points. Each constellation point carries $\log_2(K)$ bits of information.

The computational complexity of the ML detector increases with the number of constellation points, K, since it is necessary to project the observation matrix onto each and every constellation point. This is one of the main drawbacks of unstructured Grassmannian constellations especially when K is high. Another drawback of unstructured codes is how to solve the bit labeling problem, for which there are generally only suboptimal or computationally intensive solutions. In the following section we present a structured Grassmannian constellation, called *Grass-Lattice*, which solves the two problems of unstructured constellations while preserving good packing properties: it can be decoded efficiently with a computational cost that does not grow with K, and it allows for a Gray-like bit-to-symbol mapping function.

III. Grass-Lattice Constellation

A. Overview

The Grass-Lattice constellation for SIMO channels is based on a measure preserving mapping from the unit hypercube (product of the interval $(0,1)$ with itself $2(T-1)$ times) to the Grassmann manifold $\mathbb{G}\left(1,\mathbb{C}^T\right)$

$$\vartheta : \mathcal{I} = \underbrace{(0,1)\times\cdots\times(0,1)}_{2(T-1)\text{ times}} \to \mathbb{G}\left(1,\mathbb{C}^T\right),$$

where recall that $T-1$ is the complex dimension of $\mathbb{G}\left(1,\mathbb{C}^T\right)$. Elements in $\mathcal{I}$ are denoted by

$$(\mathbf{a},\mathbf{b}) = (a_1,\ldots,a_{T-1},b_1,\ldots,b_{T-1}), \quad a_k,b_k\in(0,1).$$

The Grass-Lattice mapping $\vartheta : \mathcal{I} \to \mathbb{G}\left(1,\mathbb{C}^T\right)$ has the following properties:

1) The image of ϑ is all of $\mathbb{G}\left(1,\mathbb{C}^T\right)$ except for a zero–measure subset of $\mathbb{G}\left(1,\mathbb{C}^T\right)$,
2) ϑ is a diffeomorphism onto its image,
3) and the Jacobian of ϑ is constant.

Given the mapping ϑ, if we choose a set of input points uniformly distributed in the unit hypercube, the outputs points will be uniformly distributed in $\mathbb{G}\left(1,\mathbb{C}^T\right)$. The goal is to design structured constellations that can be efficiently encoded (no need to store the constellation) and decoded (the real and imaginary parts a_j, b_j can be decoded independently). To this end, we quantize the (0,1) interval with 2^B equispaced points, where $B \geq 1$ is the number of bits per real component, and generate a Grass-Lattice constellation with $|\mathcal{C}| = 2^{2(T-1)B}$ points. The rate of the code is $R = \frac{2(T-1)B}{T}$ b/s/Hz.

The Grass-Lattice mapping is composed of three consecutive mappings $\vartheta = \vartheta_3 \circ \vartheta_2 \circ \vartheta_1$, which are described in the following subsections.

B. Mapping ϑ_1

Mapping ϑ_1 maps points uniformly distributed in the unit hypercube $\mathcal{I}$ to points normally distributed in $\mathbb{C}^{T-1}$. The idea is to apply component-wise the inverse transform sampling method, which takes uniform samples on $[0,1]$ and returns the inverse of the cumulative distribution function with the desired distribution (this is similar to the function w in the Cube-Split design, see Eq. (12) in [23]). More formally, we have the following classic result:

Lemma 1 *Let a_k, b_k be independent random variables uniformly distributed in $[0,1]$: $a_k \sim \mathcal{U}[0,1]$ and $b_k \sim \mathcal{U}[0,1]$, and let $z_k = F^{-1}(a_k) + jF^{-1}(b_k)$ where*

$$F(t) = \frac{1}{\sqrt{\pi}}\int_{-\infty}^{t} e^{-s^2}\,ds. \tag{3}$$

Then, both $\Re(z_k) = F^{-1}(a_k)$ and $\Im(z_k) = F^{-1}(b_k)$ are independent Gaussian random variables that follow a $\mathcal{N}(0,1/2)$ distribution, and hence $z_k \sim \mathcal{CN}(0,1)$.

Proof: For any integrable mapping $g : \mathbb{R} \to \mathbb{R}$, the expected value of $g(x)$ is

$$\begin{aligned}\int_0^1 g(F^{-1}(x))\,dx &= \int_{-\infty}^{\infty} g(t)|F'(t)|\,dt \\ &= \frac{1}{\sqrt{\pi}}\int_{-\infty}^{\infty} g(t)e^{-t^2}\,dt,\end{aligned}$$

where we are using the change of variables theorem. The lemma follows. □

C. Mapping ϑ_2

In Lemma 2 we describe the mapping ϑ_2, which maps normally distributed points in $\mathbb{C}^{T-1}$ to points uniformly distributed in the unit ball

$$\mathbb{B}_{\mathbb{C}^{T-1}}(0,1) = \{\mathbf{w}\in\mathbb{C}^{T-1}, \|\mathbf{w}\| < 1\}.$$

Lemma 2 *Let $\mathbf{z} = (z_1, \dots, z_{T-1})^{\mathrm{T}}$ be a $(T-1)$-dimensional Gaussian vector with i.i.d. components $z_k \sim \mathcal{CN}(0,1)$. Moreover, let*

$$f_{T-1}(t) = \frac{1}{t}\left(\frac{\gamma(T-1,t^2)}{(T-2)!}\right)^{1/(2(T-1))} = \frac{1}{t}\left(1 - e^{-t^2}\sum_{k=0}^{T-2}\frac{t^{2k}}{k!}\right)^{1/(2(T-1))}. \quad (4)$$

where $\gamma(s,x)$ represents the (lower) incomplete gamma function.
Then, the random vector $\mathbf{w} = \vartheta_2(\mathbf{z}) = \mathbf{z} f_{T-1}(\|\mathbf{z}\|)$ is uniformly distributed in the unit ball $\mathbb{B}_{\mathbb{C}^{T-1}}(0,1)$.

Proof: The proof is given in Appendix A. □

Remark 1 Since $\mathbf{z} \sim \mathcal{CN}(\mathbf{0}, \mathbf{I}_{T-1})$, $2\|\mathbf{z}\|^2 \sim \chi^2_{2(T-1)}$. The random vector $\mathbf{w} = \vartheta_2(\mathbf{z}) = \mathbf{z} f_{T-1}(\|\mathbf{z}\|)$ can be alternatively constructed as follows. Begin with the unit-norm vector $\mathbf{z}/\|\mathbf{z}\|$ that lies on $\mathcal{S}^{2(T-1)-1}$, where $d = T-1$, and scale it as

$$\mathbf{w} = \frac{\mathbf{z}}{\|\mathbf{z}\|}(F_{\chi^2_{2(T-1)}}(2\|\mathbf{z}\|^2))^{1/(2(T-1))},$$

where $F_{\chi^2_{2(T-1)}}(y)$ is the cdf of a chi-squared random variable with $2(T-1)$ degrees of freedom evaluated at y, which can be computed in closed-form as

$$F_{\chi^2_{2(T-1)}}(y) = 1 - e^{-y/2}\sum_{k=0}^{(T-1)-1}\frac{y^k}{2^k k!}.$$

The distribution of the squared norm of $\mathbf{w}$ can be derived as follows

$$\|\mathbf{w}\|^2 = \frac{\mathbf{z}^H\mathbf{z}}{\|\mathbf{z}\|^2}(F_{\chi^2_{2(T-1)}}(2\|\mathbf{z}\|^2))^{1/(T-1)} = (F_{\chi^2_{2(T-1)}}(2\|\mathbf{z}\|^2))^{1/(T-1)}.$$

Since $2\|\mathbf{z}\|^2 \sim \chi^2_{2(T-1)}$, $F_{\chi^2_{2(T-1)}}(2\|\mathbf{z}\|^2)$ is uniformly distributed in $[0,1]$. It is a known property that if $x \sim U[0,1]$ then $x^{1/r} \sim \mathrm{Beta}(r,1)$. All together, this shows that $\|\mathbf{w}\|^2 \sim \mathrm{Beta}(T-1,1)$. As a reminder, the pdf of a beta-distributed random variable with shape parameters $\alpha, \beta > 0$ is given by $f(x;\alpha,\beta) = \frac{1}{B(\alpha,\beta)}\, x^{\alpha-1}(1-x)^{\beta-1}$, where $B(\alpha,\beta) = \frac{\Gamma(\alpha)\Gamma(\beta)}{\Gamma(\alpha+\beta)}$ and $\Gamma(n) = (n-1)!$ is the Gamma function.

D. Mapping ϑ_3

In this section we present the mapping ϑ_3, which maps uniformly distributed points in the operator norm unit ball $\mathbb{B}_{\mathbb{C}^{(T-M)\times M},op}(0,1) = \{\mathbf{W} \in \mathbb{C}^{(T-M)\times M},\ \|\mathbf{W}\|_{op} < 1\}$ to points uniformly distributed in $\mathbb{G}\left(M, \mathbb{C}^T\right)$. We will first derive the mapping ϑ_3 for any value of M and then we will particularize it for $M = 1$.

Lemma 3 *Consider the mapping*

$$\begin{array}{rccc} \Theta: & \mathbb{C}^{(T-M)\times M} & \to & \mathbb{B}_{\mathbb{C}^{(T-M)\times M},op}(0,1) \\ & \mathbf{A} & \mapsto & \mathbf{A}(\mathbf{I}_M + \mathbf{A}^{\mathrm{H}}\mathbf{A})^{-1/2}, \end{array}$$

whose inverse is

$$\begin{array}{rccc} \Theta^{-1}: & \mathbb{B}_{\mathbb{C}^{(T-M)\times M},op}(0,1) & \to & \mathbb{C}^{(T-M)\times M} \\ & \mathbf{W} & \mapsto & \mathbf{W}(\mathbf{I}_M - \mathbf{W}^{\mathrm{H}}\mathbf{W})^{-1/2}. \end{array}$$

Then, the Jacobian of Θ equals $\det(\mathbf{I}_M + \mathbf{W}^{\mathrm{H}}\mathbf{W})^{-T}$.

Proof: The proof is given in Appendix B. □

We are ready to prove the following result:

Proposition 1 *For all integrable $f : \mathbb{C}^{(T-M)\times M} \to \mathbb{C}$ we have*

$$\int_{\mathbf{A}\in\mathbb{C}^{(T-M)\times M}} \frac{f(\mathbf{A})}{\det(\mathbf{I}_M + \mathbf{A}^{\mathrm{H}}\mathbf{A})^T}\, d\mathbf{A} = \int_{\substack{\mathbf{W}\in\mathbb{C}^{(T-M)\times M} \\ \|\mathbf{W}\|_{op}<1}} f\left(\mathbf{W}(\mathbf{I}_M - \mathbf{W}^{\mathrm{H}}\mathbf{W})^{-1/2}\right) d\mathbf{W}, \quad (5)$$

Proof: The proof follows from the change of variables theorem and Lemma 3 above. □

We immediately get:

Corollary 1 *For all integrable $f : \mathbb{G}(M, \mathbb{C}^T) \to \mathbb{C}$ we have*

$$\int_{[\mathbf{X}]\in\mathbb{G}(M,\mathbb{C}^T)} f([\mathbf{X}])\, d[\mathbf{X}] = \int_{\substack{\mathbf{W}\in\mathbb{C}^{(T-M)\times M} \\ \|\mathbf{W}\|_{op}<1}} f\left(\begin{bmatrix}\left(\mathbf{I}_M - \mathbf{W}^{\mathrm{H}}\mathbf{W}\right)^{1/2} \\ \mathbf{W}\end{bmatrix}\right) d\mathbf{W}. \quad (6)$$

In other words: *in order to generate a uniform random element $[\mathbf{X}]$ in $\mathbb{G}(M, \mathbb{C}^T)$, one may generate a random uniform element $\mathbf{W}$ in the operator norm unit ball of $\mathbb{C}^{(T-M)\times M}$ and output*

$$\begin{bmatrix}\left(\mathbf{I}_M - \mathbf{W}^{\mathrm{H}}\mathbf{W}\right)^{1/2} \\ \mathbf{W}\end{bmatrix}.$$

In Lemma 4 we particularize the mapping ϑ_3 for $M = 1$, which maps uniformly distributed points in the unit ball $\mathbb{B}_{\mathbb{C}^{T-1}}(0,1)$ to points uniformly distributed in $\mathbb{G}\left(1, \mathbb{C}^T\right)$. We can notice that a mapping similar to ϑ_3 for $M = 1$ has been used for the Exp-Map constellation (see Eq. (8) in [22]), despite being obtained with a completely different approach.

Lemma 4 *The mapping*

$$\begin{array}{rccc} \vartheta_3: & \mathbf{w} \in \mathbb{B}_{\mathbb{C}^{T-1}}(0,1) & \to & \mathbb{G}\left(1, \mathbb{C}^T\right) \\ & \mathbf{w} & \mapsto & \begin{bmatrix}\sqrt{1-\|\mathbf{w}\|^2} \\ \mathbf{w}\end{bmatrix} \end{array}$$

is measure preserving. So in order to generate a uniform random element $[\mathbf{x}]$ in $\mathbb{G}\left(1, \mathbb{C}^T\right)$, one may generate a random uniform element $\mathbf{w}$ in $\mathbb{B}_{\mathbb{C}^{T-1}}(0,1)$ and output $\left[\sqrt{1-\|\mathbf{w}\|^2}, \mathbf{w}^{\mathrm{T}}\right]^{\mathrm{T}}$.

E. Main result

The following theorem summarizes the measure preserving Grass-Lattice mapping for SIMO channels.

Theorem 1 *Let us consider a noncoherent SIMO communication system with coherence time $T \geq 2$ and let $(\mathbf{a}, \mathbf{b}) =$*

$(a_1, \ldots, a_{T-1}, b_1, \ldots, b_{T-1})$ be any point in the unit hypercube $\mathcal{I}$. The mapping $\vartheta : \mathcal{I} \to \mathbb{G}\left(1, \mathbb{C}^T\right)$ given by

$$\vartheta(\mathbf{a}, \mathbf{b}) = \begin{bmatrix} \sqrt{1 - \|\mathbf{w}\|^2} \\ \mathbf{w} \end{bmatrix},$$

where:

- $\mathbf{w} = \mathbf{z} f_{T-1}(\|\mathbf{z}\|)$, *where f_{T-1} is defined in* (4).
- $\mathbf{z} = (z_1, \ldots, z_{T-1})^{\mathrm{T}}$ *with* $z_k = F^{-1}(a_k) + jF^{-1}(b_k)$, *where $F(x)$ is given in* (3).

Then, ϑ has a constant Jacobian and thus it is measure preserving.

Proof: The proof is given in Appendix C. □

IV. Encoding and Decoding

For $M = 1$, the Grassmann manifold $\mathbb{G}(M, \mathbb{C}^T)$ has complex dimension $T-1$ and real dimension $2(T-1)$. Since the measure preserving map we define has domain $(0,1)^{2(T-1)}$ and $(0,1)$ is an open interval, whatever discretization we choose in $(0,1)$ will necessarily have a lowest point $\alpha > 0$ and a highest point $1 - \beta < 1$. Due to the symmetry of the mapping we find no reasons to choose $\beta \neq \alpha$ and hence for a given number B of bits per real component, we consider 2^B equispaced points on the interval $[\alpha, 1-\alpha]$:

$$\hat{x}_p = \alpha + p\,\frac{1-2\alpha}{2^B - 1}, \quad 0 \le p \le 2^B - 1, \tag{7}$$

where α is a parameter that can be optimized for performance (see Sec. V). The discretization of the real and imaginary (I/Q) components as in (7) allows us to use a simple bit-to-symbol Gray-like mapper. Therefore, the uniformly distributed points on the unit cube $a_1, b_1, \ldots, a_{T-1}, b_{T-1}$ are chosen randomly from the regular lattice defined by (7).

A. Encoder

The procedure for computing the constellation point to be transmitted $\mathbf{x}$ for an input $a_1, b_1, \ldots, a_{T-1}, b_{T-1}$ is then:

1) Compute $z_k = F^{-1}(a_k) + jF^{-1}(b_k)$, $k = 1, \ldots, T-1$, where $F(x)$ is the cdf of a $\mathcal{N}(0, 1/2)$. The point $\mathbf{z}$ is isotropically distributed as $\mathbf{z} \sim \mathcal{CN}(\mathbf{0}, \mathbf{I}_{T-1})$.
2) Compute $\mathbf{w} = \mathbf{z} f_{T-1}(\|\mathbf{z}\|)$, where $f_{T-1}(\cdot)$ is given in (4). The point $\mathbf{w}$ is uniformly distributed in $\mathbb{B}_{\mathbb{C}^{T-1}}(0,1)$.
3) Output
$$\mathbf{x} = \begin{bmatrix} \sqrt{1 - \|\mathbf{w}\|^2} \\ \mathbf{w} \end{bmatrix}.$$

The result of this procedure is a point $[\mathbf{x}]$ with representative $\mathbf{x} = \left[\sqrt{1 - \|\mathbf{w}\|^2}, \mathbf{w}^{\mathrm{T}}\right]^{\mathrm{T}}$ which is uniformly distributed in $\mathbb{G}\left(1, \mathbb{C}^T\right)$. The cardinality of the structured Grassmannian constellation is $|\mathcal{C}| = 2^{2B(T-1)}$, and the spectral efficiency or rate is $R = \frac{2B(T-1)}{T} = 2B\left(1 - \frac{1}{T}\right)$ b/s/Hz.

The input and output of the mappings ϑ_1, ϑ_2 and ϑ_3 that form the Grass-Lattice mapping can be plotted for the case $T = 2$. For this specific case, the input $(\mathbf{a}, \mathbf{b})$ has two real components (a_1, b_1) and vectors $\mathbf{z}$ and $\mathbf{w}$ have one complex component (z_1 and w_1 respectively). To represent the points $[\mathbf{x}]$ with representative $\mathbf{x} = [x_1, x_2]^{\mathrm{T}} = \left[\sqrt{1 - |w_1|^2}, w_1\right]^{\mathrm{T}}$, we use the Hopf map [29]:

$$\begin{array}{rccc} p: & \{(x_1, x_2) \in \mathbb{R} \times \mathbb{C}: & \to & \mathbb{S}^2 \\ & |x_1|^2 + |x_2|^2 = 1\} & & \\ & (x_1, x_2) & \mapsto & \left(2x_1 x_2^*, |x_2|^2 - |x_1|^2\right). \end{array} \tag{8}$$

This Hopf map is a well-known map in topology that provides an explicit smooth one-to-one representation of the projective space $\mathbb{G}(1, \mathbb{C}^2)$ into $\mathbb{S}^2$, and more generally maps higher-dimensional spheres into lower-dimensional spheres. Fig. 1 shows the generation of the whole Grass-Lattice constellation for $T = 2$, $B = 4$ and $\alpha = 0.05$.

B. Decoder

In this section we propose a greedy decoder in order to avoid the high-complexity ML decoder presented in (2). Let us first consider the case where the number of receive antennas is $N = 1$, so the received $T \times 1$ signal is $\mathbf{y} = \mathbf{x}h + \mathbf{n}$. Let $\mathbf{y} = (v_0, \mathbf{v})$, then the decoder performs the following sequence of steps:

1) Compute $\mathbf{w} = \mathbf{v}|v_0|/(v_0\|\mathbf{y}\|)$ (the chordal distance from $\left[\sqrt{1 - \|\mathbf{w}\|^2}, \mathbf{w}^{\mathrm{T}}\right]^{\mathrm{T}}$ to $\mathbf{y}$ in $\mathbb{G}(1, \mathbb{C}^T)$ is minimal for this choice of $\mathbf{w}$).
2) Solve the equation $s f_{T-1}(s) = \|\mathbf{w}\|$ by the inverse of a chi-square CDF (see Remark 1) and let $\mathbf{z} = s\mathbf{w}/\|\mathbf{w}\|$. Denote by $z_1, \ldots, z_{T-1}$ its complex components.
3) Compute $\hat{a}_k = F(\Re(z_k))$, $\hat{b}_k = F(\Im(z_k))$, where $F(x)$ is the cdf of a $\mathcal{N}(0, 1/2)$.
4) Finally, $a_k = \lfloor \hat{a}_k \rceil$ and $b_k = \lfloor \hat{b}_k \rceil$ where $\lfloor x \rceil$ denotes the nearest point to x in the lattice (7).

Multi-antenna receiver: For $N > 1$, we just perform a denoising step at the decoder before doing steps 1-4 above, which is also used in the systematic decoder of the Cube-Split constellation [23]. To do so, we use the fact that the signal of interest $\mathbf{x}\mathbf{h}^{\mathrm{T}}$ in (1) is a rank-1 component of $\mathbf{Y}$. The Eckart-Young theorem [30] states that the least squares approximation in s dimensions of an $m \times n$ matrix $\mathbf{X}$ with singular value decomposition $\mathbf{U}\mathbf{\Sigma}\mathbf{V}^H$ is obtained by replacing the smallest $n - s$ singular values of $\mathbf{\Sigma}$ with zeroes and remultiplying $\mathbf{U}\mathbf{\Sigma}\mathbf{V}^H$. Thus, the best rank-1 approximation in the Frobenius norm of $\mathbf{Y}$ is given by $\lambda_1 \mathbf{r}\mathbf{g}^{\mathrm{H}}$, where λ_1 is the largest singular value of $\mathbf{Y}$, and $\mathbf{r}$ and $\mathbf{g}$ are the corresponding left and right singular vectors. We then take $\mathbf{r} = (v_0, \mathbf{v})$ as a denoised $T \times 1$ vector of observations and compute the sequence of steps 1-4 above. Interestingly, $\mathbf{r}$ is the solution of

$$\arg \max_{\mathbf{r} \in \mathbb{C}^T:\ \|r\|^2 = 1} \|\mathbf{Y}^{\mathrm{H}}\mathbf{r}\|^2,$$

so it can be viewed as a relaxed version of the ML decoder presented in (2) where the discrete nature of the constellation has been relaxed. Therefore, $\mathbf{r}$ is a rough estimate of the transmitted symbol $\mathbf{x}$ on the unit sphere.

The encoding and decoding for the Grass-Lattice constellation can be performed on the fly, without the need to store the entire constellation. The complexity of the Grass-Lattice encoding is linear with T because of the size of the vectors

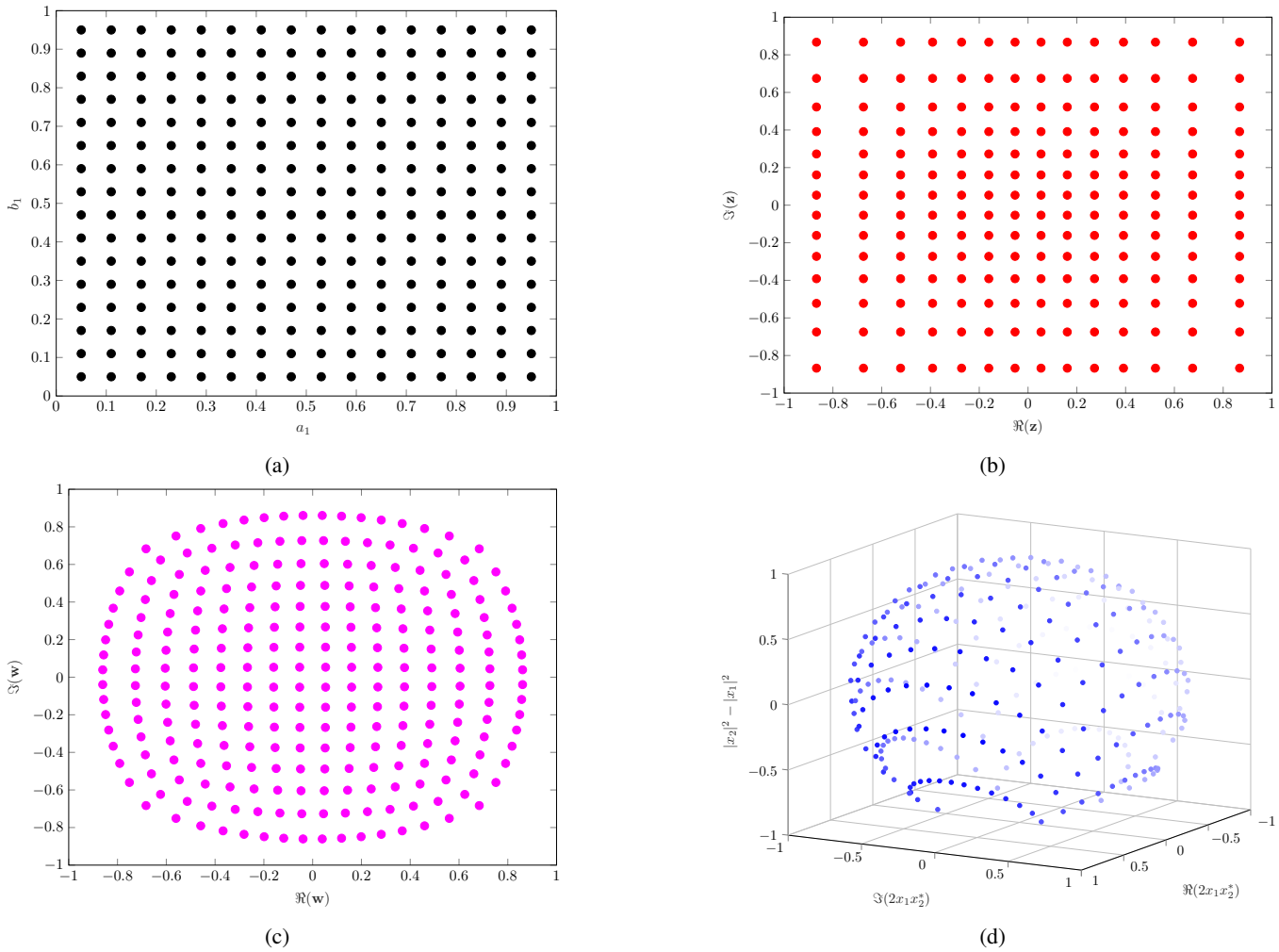

Fig. 1: Grass-Lattice mapping for $T = 2$, $B = 4$ and $\alpha = 0.05$. (a) Lattice $\mathcal{I}$. (b) Normally distributed points in $\mathbb{C}$. (c) Uniformly distributed points in $\mathbb{B}_{\mathbb{C}}(0, 1)$. (d) Uniformly distributed points in $\mathbb{G}(1, \mathbb{C}^2)$.

involved (since step 2 can be implemented as explained in Remark 1) and the complexity of the decoder is dominated by the SVD computation of the denoising step, which yields a leading complexity order of $\mathcal{O}(T^2N)$. After performing steps 1-4 above, the complexity is that of a symbol-by-symbol detector per real component, similar to the decoding of a QAM constellation.

V. Performance Evaluation

In this section, we assess the performance of the proposed Grass-Lattice constellation, and compare it to other structured and unstructured Grassmannian constellations used for non-coherent communications. Since we compare constellations with different spectral efficiencies, we will show figures of SER or BER versus E_b/N_0 (SNR normalized by the spectral efficiency).

A. SER/BER vs. α

Let us first evaluate the influence of α, which determines the length of the lattice used for each real component in (7), on the SER and the BER. Figs. 2a, 2b, 3a and 3b show the SER/BER (with the greedy decoder) vs. α curves for SNR $\in \{10, 20\}$ dB, $T \in \{4, 6\}$, $B \in \{1, 2\}$ and $N = 2$. Remember that the spectral efficiency of the Grass-Lattice constellation is $R = \frac{2(T-1)B}{T}$ b/s/Hz. As we can see, α may have a significant impact on the SER and BER performance of the Grass-Lattice constellation. Further, the SER and BER vary significantly with the number of bits, B, used to encode each real component. It is also worth noticing that the SER/BER vs. α curves are smooth functions with a unique minimum so the optimal value α^* can be easily determined by searching over a predetermined grid. Clearly, the number of bits B influences the optimal α^* more than the coherence time T. Another aspect that we observe is that the BER and SER vary similarly with α, and hence the optimal value α^* can be obtained from either the SER or BER curve. We can also see that the optimal value α^* does not change significantly with the SNR. Therefore, for the rest of experiments in this section, we will choose the value of α that provides the lowest SER at SNR = 20 dB. This value is easily precomputed offline and then used throughout the entire simulation. The optimal values of α for several values of T and B have been collected in Table I.

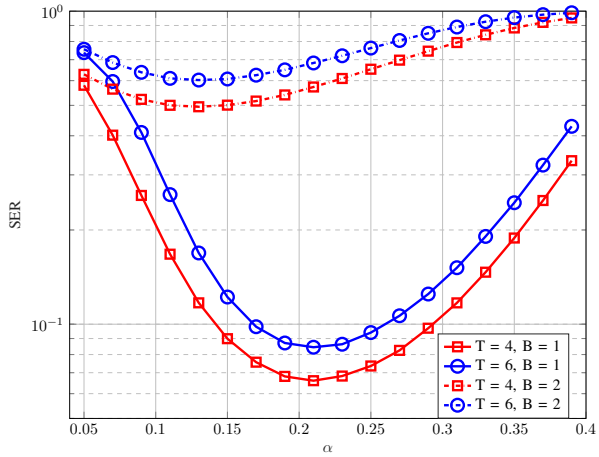

(a) SNR = 10 dB

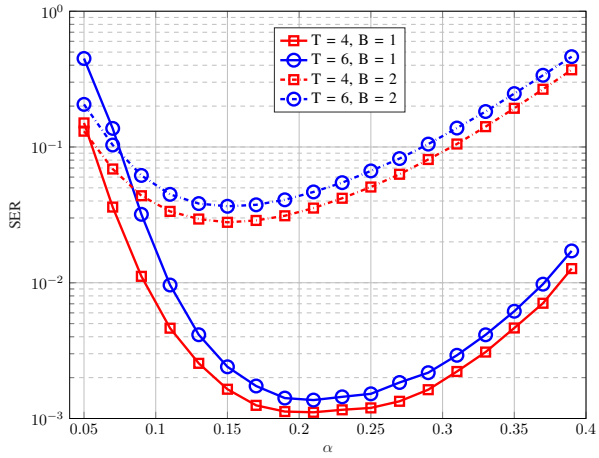

(b) SNR = 20 dB

Fig. 2: SER as a function of α of the Grass-Lattice constellation for $T \in \{4, 6\}$, $N = 2$, $B \in \{1, 2\}$ and SNR $\in \{10, 20\}$ dB.

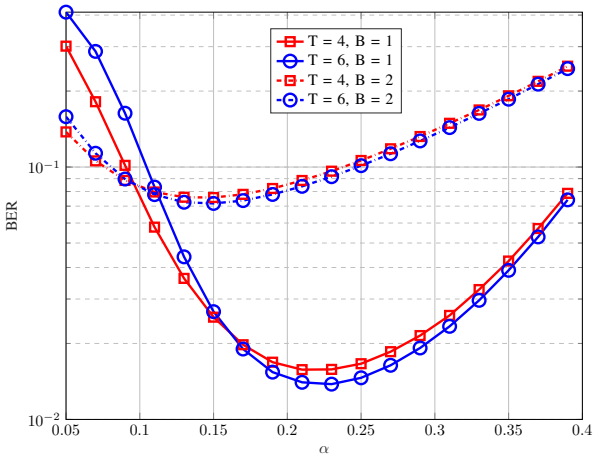

(a) SNR = 10 dB

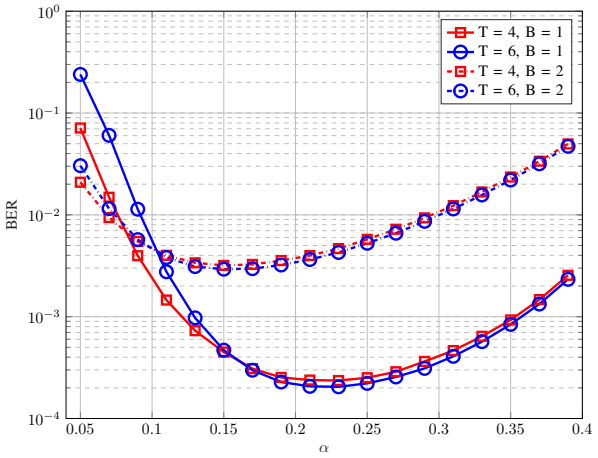

(b) SNR = 20 dB

Fig. 3: BER as a function of α of the Grass-Lattice constellation for $T \in \{4, 6\}$, $N = 2$, $B \in \{1, 2\}$ and SNR $\in \{10, 20\}$ dB.

	B = 1	**B = 2**	**B = 3**	**B = 4**	**B = 5**
T = 2	0.20	0.14	0.10	0.06	0.02
T = 3	0.20	0.14	0.10	0.05	0.03
T = 4	0.21	0.14	0.11	0.06	0.03
T = 6	0.21	0.15	0.10	0.06	0.02
T = 8	0.21	0.14	0.10	0.07	0.03
T = 14	0.22	0.14	0.11	0.07	0.03

TABLE I: Optimal values of α for different pairs (T, B).

B. Minimum chordal distance vs. α

For constellations of relatively small cardinality (up to 1024 constellation points), instead of resorting to a SER/BER simulation to calculate the optimum value of parameter α, we can generate the whole Grass-Lattice constellation and use the minimum chordal distance between points as the criterion to optimize α. In this way, α^* can be computed much faster than with the SER/BER simulation proposed in the previous section.

Fig. 4 shows the minimum chordal distance between constellation points for different values of α ranging from 0.02 to 0.4, $T = 2$ and $B \in \{2, 3, 4, 5\}$. We can observe that the functions are smooth and have a clear maximum, which gives the value of α^*. We can also see that, in this case, the optimum value of α with respect to the minimum chordal distance does not change significantly when we increase the number of bits B used to encode each real component. As the SER simulation for a fixed SNR gives a better approximation of which is the optimum value of α in practice, for the rest of experiments in this section we will choose the value of α that provides the lowest SER at SNR = 20 dB, as it was stated before.

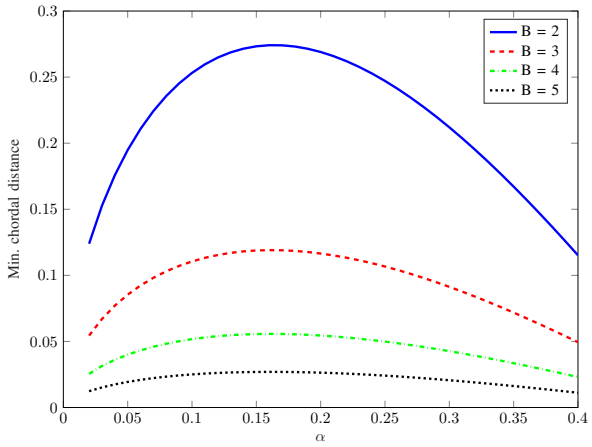

Fig. 4: Minimum chordal distance as a function of α of the Grass-Lattice constellation for $T = 2$ and $B \in \{2, 3, 4, 5\}$.

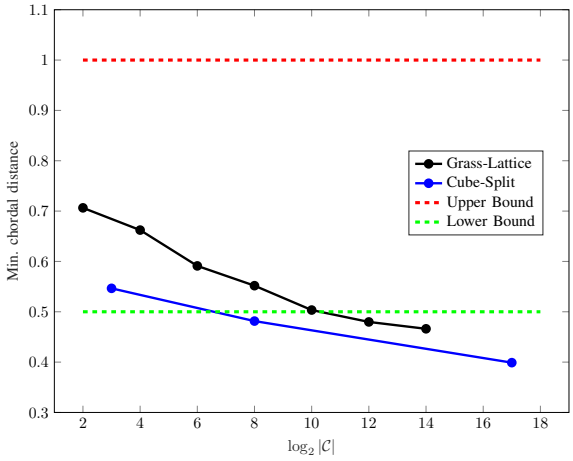

Fig. 5: Minimum chordal distance of the Grass-Lattice constellation in comparison with Cube-Split and the fundamental limits given in [23, Lem. 1] for $B = 1$.

C. Packing efficiency

Fig. 5 shows the minimum chordal distance (packing efficiency) obtained for Grass-Lattice with different constellation sizes $|\mathcal{C}|$ when $B = 1$ in comparison with Cube-Split [23]. We should recall here that for $B = 1$ the size of the Grass-Lattice constellation is given by $|\mathcal{C}| = 2^{2(T-1)}$ and the size of Cube-Split constellation is $|\mathcal{C}| = T \cdot 2^{2(T-1)}$. The packing efficiency of the proposed constellation is also benchmarked against the fundamental limits given in [23, Lem. 1]. This lemma states that the minimum distance δ of an optimal constellation of cardinality $|\mathcal{C}|$ on the complex Grassmannian of lines is bounded by

$$\min\{1, 2|\mathcal{C}|^{-\frac{1}{2(T-1)}}\} \geq \delta \geq |\mathcal{C}|^{-\frac{1}{2(T-1)}} \tag{9}$$

We observe that Grass-Lattice has a greater minimum chordal distance than Cube-Split, especially for small constellation sizes, and the packing efficiency remains between the fundamental limits for constellations with less than 1024 points.

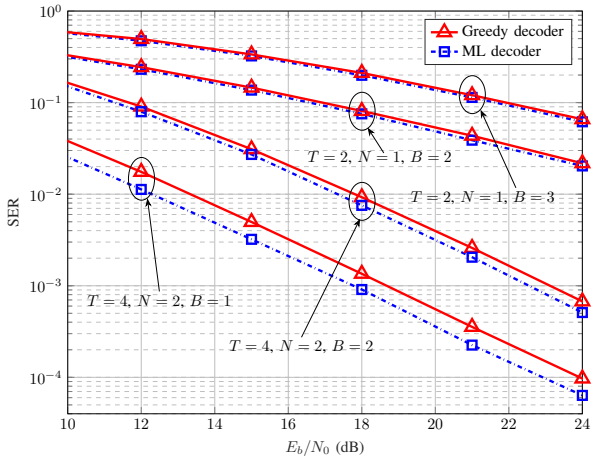

Fig. 6: SER performance of the Grass-Lattice with low-complexity greedy detector in comparison with Maximum Likelihood detector for $T \in \{2, 4\}$, $N = T/2$ and different number of bits per real component B.

D. Greedy vs. ML detector

In this section, we evaluate the SER performance of the Grass-Lattice when using two different detectors: the greedy detector proposed in Section IV-B and the optimal ML detector presented in (2). Fig. 6 shows this comparison for different scenarios with $T \in \{2, 4\}$, $N = T/2$ and different number of bits per real component B.

As we can see, in all cases the low-complexity greedy detector achieves near-ML performance, especially for those scenarios with lower coherence time T. Therefore, in the following sections we will only show the performance of the greedy detector for the Grass-Lattice constellations.

E. SER/BER vs. E_b/N_0

Fig. 7 shows the SER as a function of E_b/N_0 for the proposed Grass-Lattice constellation (with greedy decoder) for $T = 2$ symbol periods and $N = 1$ antenna. For comparison we include in the plot the structured Cube-Split [23] (with greedy decoder), Exp-Map [22] (with greedy decoder) and unitary uniquely factorable constellations (UUFC) [18] (with ML decoder), as well as the unstructured Grassmannian constellations proposed in [16] (with ML decoder) that minimize the asymptotic PEP union bound (and hence labeled as UB-Opt).

In addition, we include as a baseline the performance of a coherent pilot-based scheme. The transmitted signal for the pilot-based scheme is $\mathbf{x}_{coh} = [1, x_d]^T/\sqrt{2}$, where the first symbol is the constant pilot, which is known at the receiver, and the second symbol x_d is taken from a QAM constellation

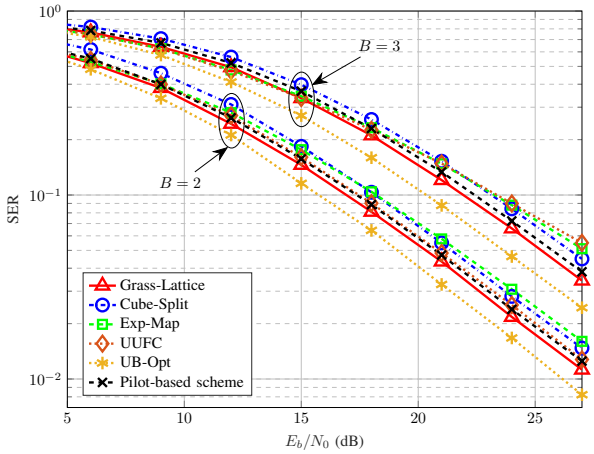

Fig. 7: Grass-Lattice SER curves in comparison with Cube-Split, Exp-Map, UUFC and UB-Opt constellations and a pilot-based scheme for $T = 2$, $N = 1$ and $B \in \{2, 3\}$.

with cardinality $2^{2(T-1)B}$, so that the coherent scheme has the same spectral efficiency as Grass-Lattice. That is, when $B = 2$ we use a 16-QAM constellation, and when $B = 3$ we use a 64-QAM constellation. The QAM constellations are normalized such that $E[|x_d|^2] = 1$. Therefore, $E[\mathbf{x}_{coh}^H \mathbf{x}_{coh}] = 1$ and hence the average transmit power of the pilot-based scheme is the same as that of the noncoherent schemes. Notice also that the power devoted to the data transmission is the same as the power devoted to training. This is the optimal power allocation for $T = 2$ and $M = 1$ as shown in [31][1].

For Grass-Lattice and Cube-Split we use $B \in \{2, 3\}$ bits per real component, while for UB-Opt, Exp-Map and UUFC we choose constellations with the same spectral efficiency as the ones provided by Grass-Lattice. In Fig. 7 we can observe that Grass-Lattice outperforms the other structured constellations and, as it was expected, it performs slightly worse than the unstructured UB-Opt constellation in terms of SER. Notice that UB-Opt uses the optimal ML detector in (2), whereas Grass-Lattice uses a suboptimal detector with much lower complexity.

Figs. 8a and 8b show the BER versus E_b/N_0 performance of Grass-Lattice constellations compared to Cube-Split, Exp-Map, weighed UB-Opt (joint constellation and bit-to-symbol mapping design) and a pilot-based scheme for $T = 2$, $N = 1$ and $B \in \{2, 3\}$. For Grass-Lattice, we use a Gray-like encoding scheme that maps groups of B bits to I/Q symbols defined in (7). A Gray-like encoder is also used for Cube-Split, Exp-Map and the pilot-based scheme. As we can see, Grass-Lattice constellations offer a superior performance in terms of BER than the other structured designs and the pilot-based scheme,

[1]In fact, it is shown in [31] that from an information-theoretic point of view using a number of pilots equal to the number of transmit antennas M is always optimal, provided that we optimize the power allocation between pilots and data. Equal power allocation is optimal for $T = 2$ and $M = 1$. Nevertheless, we should bear in mind that these results are obtained by maximizing a lower bound on the capacity. Conclusions might be different if we optimize instead the SER or BER performance.

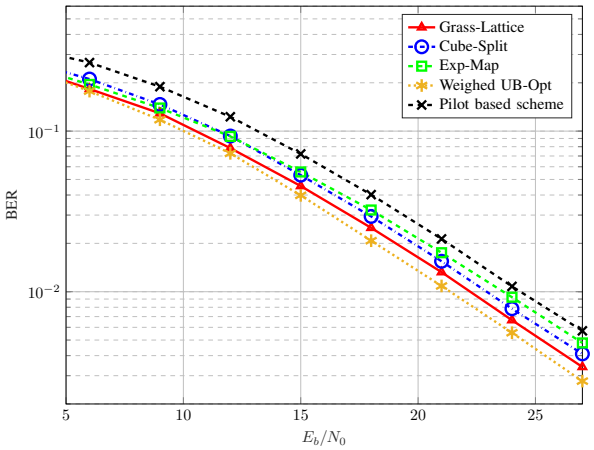

(a) $B = 2$

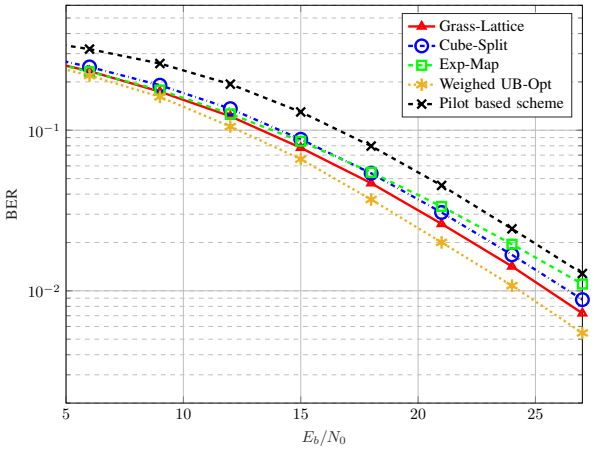

(b) $B = 3$

Fig. 8: Grass-Lattice BER curves in comparison with Cube-Split, Exp-Map and UB-Opt constellations and a pilot-based scheme for $T = 2$, $N = 1$ and $B \in \{2, 3\}$.

which becomes more evident when the coherence time T is smaller. The joint design of the unstructured constellation using the UB criterion and the bit labeling scheme provides for these examples the best performance.

In Figs. 9a and 9b we consider two different scenarios with $T = 4$, $N = 2$ and $B \in \{1, 2, 3\}$ and $T = 8$, $N = 2$ and $B \in \{1, 2\}$ respectively. We restrict the comparison for these scenarios to the Grass-Lattice, Cube-Split, and Exp-Map. Although Grass-Lattice is still the best performing method, the differences with Cube-Split are reduced, especially for a small number of bits.

F. Spectral efficiency vs. E_b/N_0

Finally, Fig. 10 shows the spectral efficiency or rate in b/s/Hz against E_b/N_0 at BER=10^{-4} for different values of T and $N = 2$ for the Grass-Lattice and Cube-Split constellations.

For given values of T and B, the spectral efficiency

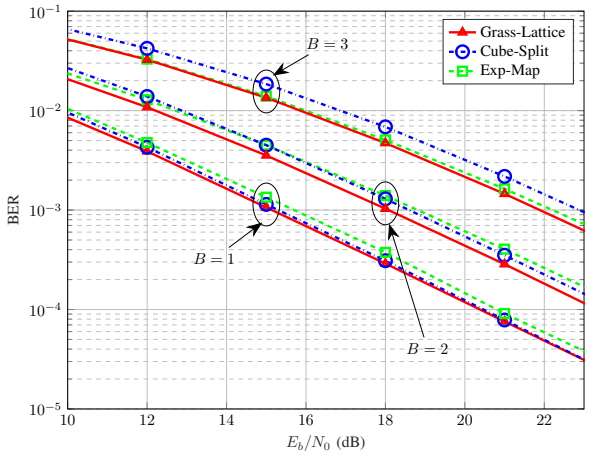

(a) $T = 4$, $B \in \{1, 2, 3\}$

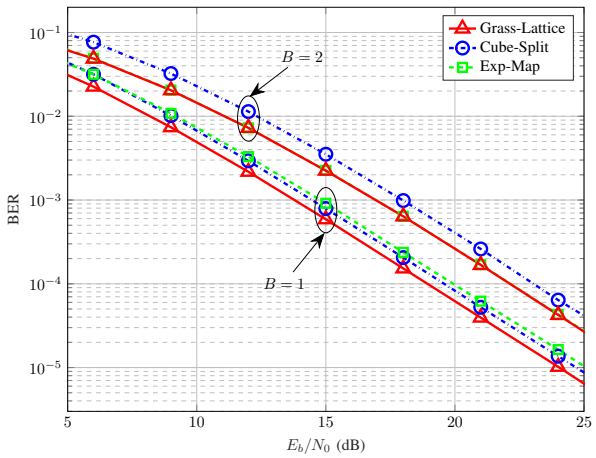

(b) $T = 8$, $B \in \{1, 2\}$

Fig. 9: Grass-Lattice BER curves in comparison with Cube-Split and Exp-Map constellations for $T \in \{4, 8\}$, $N = 2$ and different number of bits per real component B.

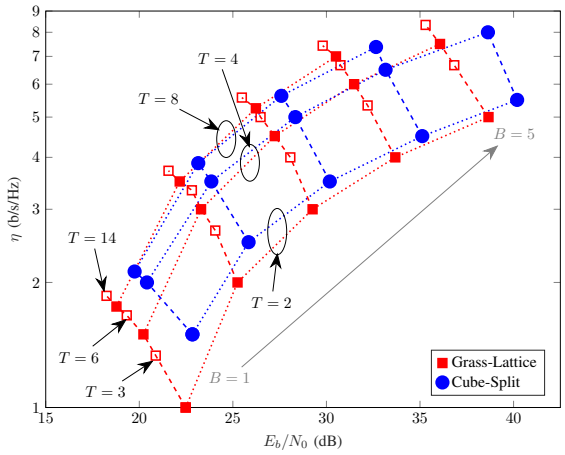

Fig. 10: Spectral efficiency of Grass-Lattice and Cube-Split as a function of E_b/N_0 at 10^{-4} BER for $T \in \{2, 3, 4, 6, 8, 14\}$ and $N = 2$.

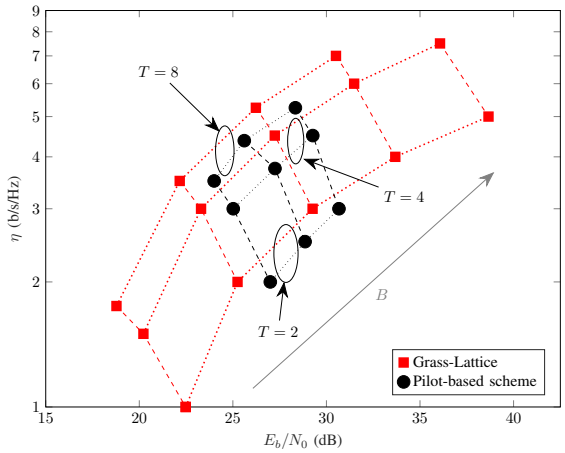

Fig. 11: Spectral efficiency of Grass-Lattice and a pilot-based scheme as a function of E_b/N_0 at 10^{-4} BER for $T \in \{2, 4, 8\}$ and $N = 2$.

of the Grass-Lattice code is $\eta = (2B(T-1))/T$ and the spectral efficiency of Cube-split is given by $\eta = (\log_2 T + 2B(T-1))/T$. We notice from these two expressions that Cube-Split does not allow for a bit-to-symbol mapping when T is not a power of 2, so Grass-Lattice achieves a wider range of spectral efficiencies. For example, we can see in this figure that Grass-Lattice allows you to design constellations for $T \in \{3, 6, 14\}$. For values of $T \in \{2, 4, 8\}$, for which Grass-Lattice and Cube-Split constellations can be both designed, we see that Grass-Lattice is more power efficient than Cube-Split when T or B grows. This could be at least partially explained by the fact that Cube-Split ignores the statistical dependencies between the different components of the constellation point $\mathbf{x}$ for $T > 2$.

Fig. 11 shows a comparison between Grass-Lattice and a coherent pilot-based scheme. For the coherent scheme for each value of T we get three points that correspond to transmissions with 16-QAM, 32-QAM and 64-QAM signals. In all cases, the optimal number of pilots to send is 1, and the power allocation between the pilot and the data has been optimized according to [31]. We have used the MMSE channel estimator and the MMSE decoder. The figure clearly shows the spectral efficiency improvement of Grass-Lattice over the pilot-based scheme.

VI. Conclusion

We have proposed a new Grassmannian constellation for noncoherent communications in SIMO channels, named Grass-Lattice, based on a measure preserving mapping from the unit hypercube to the Grassmannian of lines. Thanks to its structure, the encoding and decoding steps can be performed on the fly with no need to store the whole constellation. Further, it allows for low-complexity and efficient decoding

as well as for a simple Gray-like bit labeling. Simulation results show that Grass-Lattice has symbol and bit error rate performance close to that of a numerically optimized unstructured constellation. Besides, the designed constellations outperform other structured constellations in the literature and a coherent pilot-based scheme in terms of SER and BER under Rayleigh block fading channels, in addition to being more power efficient. As mappings ϑ_1 and ϑ_3 have already been derived in this paper for any number of transmit antennas, further research will be done to study the extension of mapping ϑ_2 and, consequently, the whole Grass-Lattice mapping, to the MIMO case.

APPENDIX

A. Proof of Lemma 2

Let us define $d = T - 1$. The function f_d is the unique solution of

$$f(t)^{2d-1}(f(t) + tf'(t)) = \frac{e^{-t^2}}{\Gamma(d+1)}, \quad \lim_{t\to\infty} tf(t) = 1,$$

which satisfies $tf(t) \in [0, 1)$ and can be written in terms of an incomplete Gamma function. It is easy to see that $\vartheta_2 : \mathbb{C}^d \to \mathbb{B}_{\mathbb{C}^d}(0, 1)$ is a diffeomorphism. Let us compute the Jacobian of ϑ_2: if $\dot{\mathbf{z}}$ is (real) orthogonal to $\mathbf{z}$ then

$$D\vartheta_2(\mathbf{z})\dot{\mathbf{z}} = \dot{\mathbf{z}} f_d(\|\mathbf{z}\|),$$

while for $\dot{\mathbf{z}} = \mathbf{z}/\|\mathbf{z}\|$ we have

$$\begin{aligned} D\vartheta_2(\mathbf{z})\frac{\mathbf{z}}{\|\mathbf{z}\|} &= \frac{\mathbf{z}}{\|\mathbf{z}\|} f_d(\|\mathbf{z}\|) + \mathbf{z} f_d'(\|\mathbf{z}\|) \\ &= \mathbf{z}\left(\frac{f_d(\|\mathbf{z}\|)}{\|\mathbf{z}\|} + f_d'(\|\mathbf{z}\|)\right). \end{aligned}$$

Choosing any orthonormal basis of $\mathbb{C}^d \equiv \mathbb{R}^{2d}$ whose last vector is $\mathbf{z}/\|\mathbf{z}\|$ we thus have that the orthogonality of this basis is preserved by $D\vartheta_2$. The Jacobian of ϑ_2 at $\mathbf{z}$ is then just the product of the lengths of the resulting vectors:

$$Jac\,\vartheta_2(\mathbf{z}) = f_d(\|\mathbf{z}\|)^{2d-1}(f(\|\mathbf{z}\|)+\|\mathbf{z}\|f'(\|\mathbf{z}\|)) = \frac{e^{-\|\mathbf{z}\|^2}}{\Gamma(d+1)}.$$

Given any integrable mapping $g : \mathbb{B}_{\mathbb{C}^d}(0, 1) \to \mathbb{R}$, the expected value of $g(\mathbf{w})$ when $\mathbf{w}$ follows the distribution of the lemma is:

$$\begin{aligned} I &= \frac{1}{\pi^d}\int_{\mathbf{z}\in\mathbb{C}^d} g(\vartheta_2(\mathbf{z}))e^{-\|\mathbf{z}\|^2}\, d\mathbf{z} \\ &= \frac{\Gamma(d+1)}{\pi^d}\int_{\mathbf{z}\in\mathbb{C}^d} g(\vartheta_2(\mathbf{z}))Jac\,\vartheta_2(\mathbf{z})\, d\mathbf{z}, \end{aligned}$$

which by the Change of Variables Theorem equals

$$\frac{\Gamma(d+1)}{\pi^d}\int_{\mathbf{w}\in\mathbb{B}_{\mathbb{C}^d}(0,1)} g(\mathbf{w})\, d\mathbf{w}.$$

This is the expected value of g in $\mathbb{B}_{\mathbb{C}^d}(0, 1)$, since the volume of $\mathbb{B}_{\mathbb{C}^d}(0, 1)$ is precisely $\pi^d/\Gamma(d + 1)$.

B. Proof of Lemma 3

That the formula for Θ^{-1} is the claimed one is easy to see: just write down the singular value decomposition of $\mathbf{W} = \mathbf{U}\binom{\mathbf{D}}{\mathbf{0}}\mathbf{V}^{\mathrm{H}}$ and compose the two functions in any order to see that you get the identity map in each space. Now let us compute the Jacobian. First, note that for any given unitary $T \times T$ matrix $\mathbf{U}$ the isometry $\mathbf{A} \to \mathbf{UA}$ in the domain commutes with the isometry $\mathbf{B} \to \mathbf{UB}$ in the range, and the same happens with the isometry $\mathbf{A} \to \mathbf{AV}$ if $\mathbf{V}$ is unitary of size M. It suffices to prove our result in the case that $\mathbf{A} = \binom{\mathbf{D}}{\mathbf{0}}$ with $\mathbf{D} = \mathrm{diag}(\sigma_1, \ldots, \sigma_M)$. Let us compute the corresponding directional derivatives:

- For $\dot{\mathbf{A}} = \binom{\mathbf{0}}{\dot{\mathbf{C}}}$ we have

$$\begin{aligned} D\Theta(\mathbf{A})(\dot{\mathbf{A}}) = \frac{d}{dt}\,|_{t=0} \Bigg(\binom{\mathbf{D}}{t\dot{\mathbf{C}}}\Big(\mathbf{I}_M + \begin{pmatrix}\mathbf{D} & t\dot{\mathbf{C}}^{\mathrm{H}}\end{pmatrix} \\ \cdot \binom{\mathbf{D}}{t\dot{\mathbf{C}}}\Big)^{-1/2}\Bigg) \\ = \binom{\mathbf{0}}{\dot{\mathbf{C}}}(\mathbf{I}_M + \mathbf{D}^2)^{-1/2}. \end{aligned}$$

  The natural basis for $\dot{\mathbf{C}}$ then preserves orthogonality and this yields a factor for the Jacobian of Θ of:

$$\prod_{m=1}^{M} \frac{1}{(1+\sigma_m^2)^{T-2M}} = \det(\mathbf{I}_M + \mathbf{A}^{\mathrm{H}}\mathbf{A})^{-T+2M}.$$

- If $\dot{\mathbf{A}} = \binom{\boldsymbol{\delta}_{kk}}{\mathbf{0}}$, where $\boldsymbol{\delta}_{kk}$ denotes an $M \times M$ matrix whose only nonzero term δ_{kk} is located at row k and column k, then a direct computation shows that

$$D\Theta(\mathbf{A})(\dot{\mathbf{A}}) = \frac{1}{(1+\sigma_k^2)^{3/2}},$$

  and similarly if $\dot{\mathbf{A}} = \binom{j\delta_{kk}}{\mathbf{0}}$ then

$$D\Theta(\mathbf{A})(\dot{\mathbf{A}}) = j\frac{1}{(1+\sigma_k^2)^{1/2}},$$

  which again preserves orthogonality and adds the following factor to the Jacobian of Θ

$$\prod_{m=1}^{M} \frac{1}{(1+\sigma_m^2)^{2}} = \det(\mathbf{I}_M + \mathbf{A}^{\mathrm{H}}\mathbf{A})^{-2}$$

- If $\dot{\mathbf{A}} = \binom{\boldsymbol{\delta}_{12}}{\mathbf{0}}$, denoting $R = \sqrt{(1+\sigma_1^2)(1+\sigma_2^2)}$ then we have

$$\begin{aligned} D\Theta(\mathbf{A})(\dot{\mathbf{A}}) = \frac{d}{dt}\,|_{t=0} \Bigg(\binom{\mathbf{D}+t\delta_{12}}{0}\big(\mathbf{I}_M + (\mathbf{D}+t\delta_{21}) \\ \cdot (\mathbf{D}+t\delta_{12})\big)^{-1/2}\Bigg) \\ = \frac{1}{R\sqrt{2+\sigma_1^2+\sigma_2^2+2R}} \\ \cdot \begin{pmatrix} 0 & 1+R & & & \\ -\sigma_1\,\sigma_2 & 0 & & & \\ & & 0 & & \\ & & & \ddots & \\ & & & & 0 \end{pmatrix}, \end{aligned}$$

while if $\dot{\mathbf{A}} = \binom{\boldsymbol{\delta}_{21}}{0}$ then we have

$$D\Theta(\mathbf{A})(\dot{\mathbf{A}}) = \frac{d}{dt}\,|_{t=0} \left(\begin{pmatrix} \mathbf{D} + t\delta_{21} \\ 0 \end{pmatrix} \big(\mathbf{I}_M + (\mathbf{D} + t\delta_{12}) \cdot (\mathbf{D} + t\delta_{21})\big)^{-1/2} \right)$$

$$= \frac{1}{R\sqrt{2+\sigma_1^2+\sigma_2^2+2R}} \cdot \begin{pmatrix} 0 & -\sigma_1\,\sigma_2 & & & \\ 1+R & 0 & & & \\ & & 0 & & \\ & & & \ddots & \\ & & & & 0 \end{pmatrix},$$

Hence, the volume of the parallelepiped spanned by these two vectors is

$$\frac{(1+R)^2 - \sigma_1^2\sigma_2^2}{R^2(2+\sigma_1^2+\sigma_2^2+2R} = \frac{1}{R^2}.$$

This yields a factor $\frac{1}{(1+\sigma_1^2)(1+\sigma_2^2)}$ for the Jacobian. The same computation for $\boldsymbol{\delta}_{ij}$ gives all together:

$$\prod_{m=1}^{M} \frac{1}{(1+\sigma_m^2)^{M-1}} = \det(\mathbf{I}_M + \mathbf{A}^{\mathrm{H}}\mathbf{A})^{-(M-1)}$$

- If $\dot{\mathbf{A}} = \binom{\mathrm{j}\boldsymbol{\delta}_{12}}{\mathbf{0}}$ and later $\dot{\mathbf{A}} = \binom{\mathrm{j}\boldsymbol{\delta}_{21}}{\mathbf{0}}$ we get the same computation, which yields another factor of

$$\prod_{m=1}^{M} \frac{1}{(1+\sigma_m^2)^{M-1}} = \det(\mathbf{I}_M + \mathbf{A}^{\mathrm{H}}\mathbf{A})^{-(M-1)}.$$

Multiplying all the factors, we have that the Jacobian of Θ is $\det(\mathbf{I}_M + \mathbf{A}^{\mathrm{H}}\mathbf{A})^{-T}$. This finishes the proof.

C. Proof of Theorem 1

Let $G : \mathbb{G}\left(1, \mathbb{C}^T\right) \to \mathbb{C}$ be integrable. From Lemma 1,

$$\frac{1}{Vol(\mathbb{G}\left(1,\mathbb{C}^T\right))} \int_{[\mathbf{x}]\in\mathbb{G}(1,\mathbb{C}^T)} G([\mathbf{x}])\, d[\mathbf{x}]$$
$$= \frac{1}{Vol(\mathbb{B}_{\mathbb{C}^{T-1}}(0,1))} \int_{\substack{\mathbf{w}\in\mathbb{C}^{T-1} \\ \|\mathbf{w}\|<1}} G\left(\begin{bmatrix} \sqrt{1-\|\mathbf{w}\|^2} \\ \mathbf{w} \end{bmatrix}\right) d\mathbf{w},$$

where $Vol(\mathbb{S})$ denotes the volume of the set $\mathbb{S}$. From Lemma 2, this equals

$$\frac{1}{\pi^{T-1}} \int_{\mathbf{z}\in\mathbb{C}^{T-1}} G\left(\begin{bmatrix} \sqrt{1-\|\mathbf{z}f_{T-1}(\|\mathbf{z}\|)\|^2} \\ \mathbf{z}f_{T-1}(\|\mathbf{z}\|) \end{bmatrix}\right) e^{-\|\mathbf{z}\|^2}\, d\mathbf{z},$$

which in turn from Lemma 1 equals

$$\int_{(\mathbf{a},\mathbf{b})\in\mathcal{I}} G\left(\begin{bmatrix} \sqrt{1-\|\mathbf{z}f_{T-1}(\|\mathbf{z}\|)\|^2} \\ \mathbf{z}f_{T-1}(\|\mathbf{z}\|) \end{bmatrix}\right) d(\mathbf{a},\mathbf{b}),$$

where

$$\mathbf{z} = (z_1, \ldots, z_{T-1})^{\mathrm{T}}, \quad z_k = F^{-1}(a_k) + jF^{-1}(b_k).$$

All in one, we have proved that the point

$$\begin{bmatrix} \sqrt{1-\|\mathbf{w}\|^2} \\ \mathbf{w} \end{bmatrix}$$

with $\mathbf{w} = \mathbf{z}f_{T-1}(\|\mathbf{z}\|)$, is uniformly distributed in $\mathbb{G}\left(1, \mathbb{C}^T\right)$.

REFERENCES

[1] E. Telatar, "Capacity of multi-antenna Gaussian channels," *European Transactions on Telecommunications*, vol. 10, pp. 585–595, Dec. 1999.

[2] G. Foschini and M. Gans, "On limits of wireless communications in a fading environment when using multiple antennas," *Wireless Personal Communications*, vol. 6, pp. 311–335, Mar. 1998.

[3] X.-C. Gao, J.-K. Zhang, H. Chen, Z. Dong, and B. Vucetic, "Energy-efficient and low-latency massive SIMO using noncoherent ML detection for industrial IoT communications," *IEEE Internet of Things Journal*, vol. 6, pp. 6247–6261, Aug. 2019.

[4] S. Li, Z. Dong, H. Chen, and X. Guo, "Constellation design for noncoherent massive SIMO systems in URLLC applications," *IEEE Transactions on Communications*, vol. 69, pp. 4387–4401, July 2021.

[5] T. Marzetta and B. Hochwald, "Capacity of a mobile multiple-antenna communication link in Rayleigh flat fading," *IEEE Transactions on Information Theory*, vol. 45, pp. 139–157, Jan. 1999.

[6] B. Hochwald and T. Marzetta, "Unitary space-time modulation for multiple-antenna communication in Rayleigh flat-fading," *IEEE Transactions on Information Theory*, vol. 46, pp. 1962–1973, Mar. 2000.

[7] L. Zheng and D. Tse, "Communication on the Grassmann manifold: a geometric approach to the noncoherent multiple-antenna channel," *IEEE Transactions on Information Theory*, vol. 48, pp. 359–383, Feb. 2002.

[8] J. H. Conway, R. H. Hardin, and N. J. A. Sloane, "Packing lines, planes, etc.: Packings in Grassmannian spaces," *Experimental Mathematics*, vol. 5, pp. 139–159, Apr. 1996.

[9] W. Zhao, G. Leus, and G. B. Giannakis, "Orthogonal design of unitary constellations for uncoded and trellis-coded noncoherent space-time systems," *IEEE Transactions on Information Theory*, vol. 50, pp. 1319–1327, June 2004.

[10] I. S. Dhillon, R. W. Heath Jr., T. Strohmer, and J. A. Tropp, "Constructing packings in Grassmannian manifolds via alternating projection," *Experimental Mathematics*, vol. 17, Oct. 2007.

[11] M. Beko, J. Xavier, and V. A. N. Barroso, "Noncoherent communications in multiple-antenna systems: receiver design and codebook construction," *IEEE Transactions on Signal Processing*, vol. 55, pp. 5703–5715, Dec. 2007.

[12] R. H. Gohary and T. N. Davidson, "Noncoherent MIMO communication: Grassmannian constellations and efficient detection," *IEEE Transactions on Information Theory*, vol. 55, pp. 1176–1205, Mar. 2009.

[13] D. Cuevas, C. Beltrán, I. Santamaria, V. Tuček, and G. Peters, "A fast algorithm for designing Grassmannian constellations," in *25th International ITG Workshop on Smart Antennas (WSA 2021)*, (EURECOM, France), Nov. 2021.

[14] J. Álvarez-Vizoso, D. Cuevas, C. Beltrán, I. Santamaria, V. Tuček, and G. Peters, "Coherence-based subspace packings for MIMO noncoherent communications," in *30th European Signal Processing Conference (EUSIPCO 2022)*, (Belgrade, Serbia), Aug. 2022.

[15] M. L. McCloud, M. Brehler, and M. Varanasi, "Signal design and convolutional coding for noncoherent space-time communication on the block-Rayleigh-fading channel," *IEEE Transactions on Information Theory*, vol. 48, pp. 1186–1194, May 2002.

[16] D. Cuevas, J. Álvarez-Vizoso, C. Beltrán, I. Santamaria, V. Tuček, and G. Peters, "Union bound minimization approach for designing Grassmannian constellations," *IEEE Transactions on Communications*, vol. 71, pp. 1940–1952, Apr. 2023.

[17] B. Hochwald, T. Marzetta, T. J. Richardson, W. Sweldens, and R. Urbanke, "Systematic design of unitary space-time constellations," *IEEE Transactions on Information Theory*, vol. 48, pp. 1962–1973, Sept. 2000.

[18] S. Li, J.-K. Zhang, and X. Mu, "Design of optimal noncoherent constellations for SIMO systems," *IEEE Transactions on Communications*, vol. 67, pp. 5706–5720, Aug. 2019.

[19] M. Soleymani and H. Mahdavifar, "Analog subspace coding: A new approach to coding for non-coherent wireless networks," *IEEE Transactions on Information Theory*, vol. 68, pp. 2349–2364, Apr. 2022.

[20] B. Hughes, "Differential space-time modulation," *IEEE Transactions on Information Theory*, vol. 46, pp. 2567–2578, Nov. 2000.

[21] R. Pitaval and O. Tirkkonen, "Grassmannian packings from orbits of projective group representations," in *46th Asilomar Conference on Signals, Systems and Computers (Asilomar 2012)*, (Pacific Grove, CA, USA), pp. 478–482, Nov. 2012.

[22] I. Kammoun, A. M. Cipriano, and J. Belfiore, "Non-coherent codes over the Grassmannian," *IEEE Transactions on Wireless Communications*, vol. 6, pp. 3657–3667, Oct. 2007.

[23] K. Ngo, A. Decurninge, M. Guillaud, and S. Yang, "Cube-split: A structured Grassmannian constellation for non-coherent SIMO commu-

nications," *IEEE Transactions on Wireless Communications*, vol. 19, pp. 1948–1964, Mar. 2020.
[24] J. Fanjul, I. Santamaria, and C. Loucera, "Experimental evaluation of non-coherent MIMO Grassmannian signaling schemes," in *16th International Conference on Ad Hoc Networks and Wireless (AdHoc-Now 2017)*, (Messina, Italy), Sept. 2017.
[25] G. Han and J. Rosenthal, "Geometrical and numerical design of structured unitary space-time constellations," *IEEE Transactions on Information Theory*, vol. 52, pp. 3722–3735, Aug. 2006.
[26] H. Shi, H. Zhang, G. Li, and X. Wang, "Stable embedding of Grassmann manifold via Gaussian random matrices," Feb. 2014.
[27] D. Cuevas, J. Álvarez-Vizoso, C. Beltrán, I. Santamaria, V. Tuček, and G. Peters, "A measure preserving mapping for structured Grassmannian constellations in SIMO channels," in *2022 IEEE Global Communications Conference: Signal Processing for Communications (Globecom 2022 SPC)*, (Rio de Janeiro, Brazil), Dec. 2022.
[28] D. Ramírez, I. Santamaria, and L. L. Scharf, *Coherence in Signal Processing and Machine Learning*. Springer, July 2022.
[29] D. W. Lyons, "An elementary introduction to the Hopf fibration," *Mathematics Magazine*, vol. 76, pp. 87–98, Apr. 2003.
[30] C. Eckart and G. Young, "The approximation of one matrix by another of lower rank," *Psychometrika*, vol. 1, pp. 211–218, Sept. 1936.
[31] B. Hassibi and B. M. Hochwald, "How much training is needed in multiple-antenna wireless links," *IEEE Transactions on Information Theory*, vol. 49, pp. 951–963, Apr. 2003.

Diego Cuevas received the B.E. degree in telecommunications engineering from the Universidad de Cantabria (UC), Spain, in 2018, and the M.Sc. degree in telecommunications engineering from the Universidad de Cantabria, Spain, in 2020. In October 2020, he joined the Department of Communications Engineering, Universidad de Cantabria, where he is currently working toward the Ph.D. degree in electrical engineering. His current research interests include noncoherent wireless communications, signal processing algorithms for multiple-antenna wireless communications and machine learning.

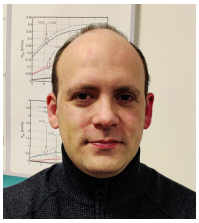

Javier Álvarez-Vizoso received his Licenciatura degree in Physics at Universidad de Oviedo, Spain, in 2013, and graduated with a Ph.D. in mathematics at Colorado State University, USA, in 2018. He has held a postdoctoral position in applied mathematics at the Max Planck Institute of Solar System Research, Germany. In October 2021 he joined the Department of Communications Engineering, Universidad de Cantabria, as postdoctoral fellow, where he is currently working for the Advanced Signal Processing Group. His research interests range from Riemannian optimization to machine learning and their applications to communications.

Carlos Beltrán received the Ph.D. degree in mathematics from the Universidad de Cantabria (UC), Spain, in 2006. He held a Postdoctoral Fellowship at the University of Toronto during 2007 and 2008, and is currently Full Professor on Mathematical Analysis at the Universidad de Cantabria. He has published over 40 research papers including some which describe a probabilistic solution to Smale's 17th problem and other well-known open problems in the frontiers of Mathematics and Computation. His research interests include numerical analysis, complexity and approximation theory, as well as applied problems. He received the Jose Luis Rubio de Francia 2010 prize (Real Sociedad Matemática Española) and the Stephen Smale 2014 prize (Society for the Foundations of Computational Mathematics) for his contributions. He has delivered more than 50 talks including several plenaries at different international conferences.

Ignacio Santamaria (M'96–SM'05) received the Telecommunication Engineer degree and the Ph.D. degree in electrical engineering from the Universidad Politécnica de Madrid (UPM), Spain, in 1991 and 1995, respectively. Since 2007 he is Full Professor at the Universidad de Cantabria (UC). He has coauthored the book "Coherence in Signal Processing and Machine Learning", Springer, 2022, and more than 200 publications in refereed journals and international conference papers. His research interests include signal processing algorithms and information-theoretic aspects of multiuser multiantenna wireless communication systems, multivariate statistical techniques and machine learning theories. He has been involved in numerous national and international research projects on these topics. He has been a visiting researcher at the University of Florida (in 2000 and 2004), at the University of Texas at Austin (in 2009), and at the Colorado State University (in 2015). Prof. Santamaria was General Co-Chair of the 2012 IEEE Workshop on Machine Learning for Signal Processing (MLSP 2012). He has been a member of the IEEE Machine Learning for Signal Processing Technical Committee (2009-2014), member of the IEEE Signal Processing Theory and Methods (SPTM) Technical Committee (2020-2022), and member of the IEEE Data Science Initiative (DSI) steering committee (2020-2022). He has been Associate Editor of the IEEE Transactions on Signal Processing (2011-2015), and Senior Area Editor of the IEEE Transactions on Signal Processing (2013-2015). Prof. Santamaria was a co-recipient of the 2008 EEEfCOM Innovation Award for the development of a new RF-MIMO transceiver, coauthor of a paper that received the 2012 IEEE Signal Processing Society Young Author Best Paper Award, and he has recently received the 2022 IHP International Wolfgang Mehr Fellowship Award.

Vít Tuček received his PhD degree in differential geometry and global analysis at the Charles University in Prague, Czech Republic in 2017. In 2018 he joined the Scientific Center of Excellence for Quantum and Complex Systems, and Representations of Lie Algebras (QuantiXLie) at the University of Zagreb, Croatia. Currently he is affiliated with Huawei Sweden R&D where he works on non-coherent communication schemes. His main focus are homogeneous spaces and related representation theory.

Gunnar Peters received the Ph.D. degree in mathematics and the Master of Engineering degree in applied physics from the Royal Institute of Technology. He is a Senior Expert of Network Algorithms with Huawei, Sweden. He has worked in telecom for 19 years and started with Ericsson in 2000, where he was an Expert in Radio Performance. In 2010, he joined the Wireless Organization, Huawei, where he is the Director of Wireless Network Algorithm Lab. He has also worked with the University of South Carolina, Uppsala University, and the Royal Institute of Technology. His research covers stochastic state mechanics, signal processing, and radio resource management. He has received the Individual Gold Medal Award and the Team Gold Medal Award for his work in massive MIMO, advanced receivers, and the application of machine learning to RAN.